Supporting Information

Manuscript Title:

Synthesis and characterization of ^{15}N-labeled tetranuclear Ir complexes *via* $Li_2C^{15}N_2$

Authors:

Xuechao Yan,[a] Shu-Xiao Ji,[a] Shengyuan Zhang,[bc] Qianru Wang,[bc*] Jianping Guo,[bc] Ping Chen,[bc] Zhenfeng Xi,[ad] and Junnian Wei [a*]

Affiliations:

[a] Beijing National Laboratory for Molecular Sciences (BNLMS), Key Laboratory of Bioorganic Chemistry and Molecular Engineering of Ministry of Education, College of Chemistry, Peking University, Beijing 100871, China.

[b] Dalian Institute of Chemical Physics, Chinese Academy of Sciences, Dalian 116023, China.

[c] Center of Materials Science and Optoelectronics Engineering, University of Chinese Academy of Sciences, Beijing 100049, China.

[d] State Key Laboratory of Organometallic Chemistry, Shanghai Institute of Organic Chemistry, Shanghai 200032, China

Contents:

1) Copies of NMR Spectra

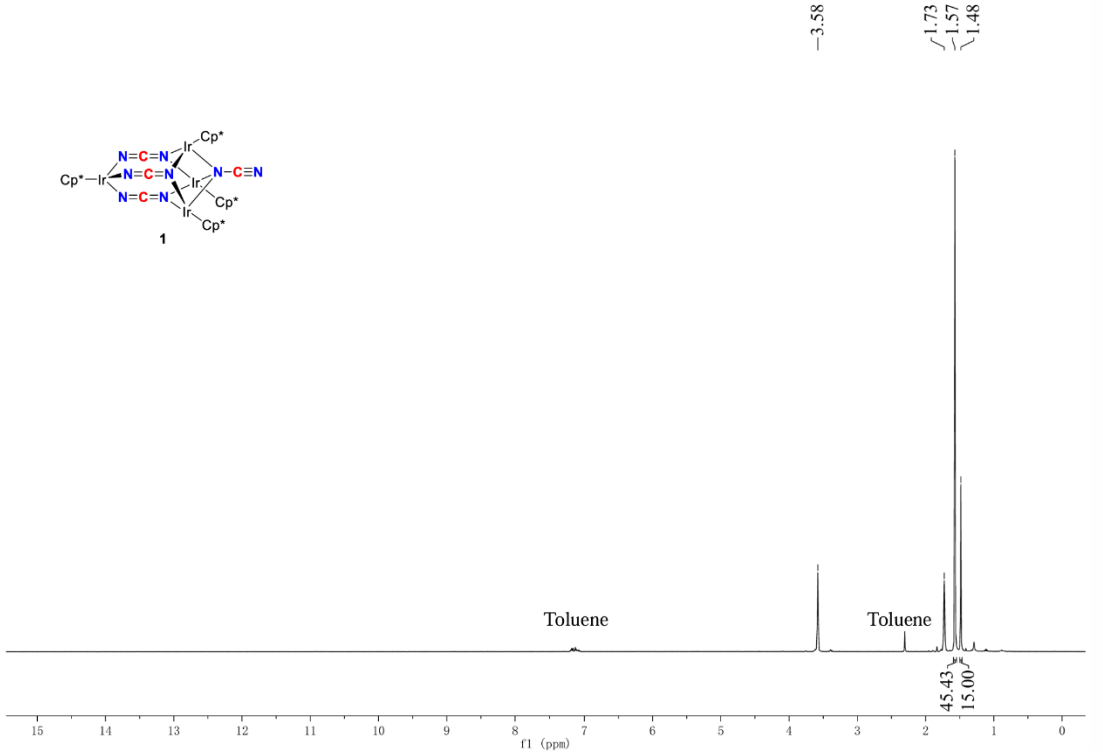

Figure S1. ^{1}H NMR spectrum of **1** (25 °C, 400 MHz, d_8-THF).

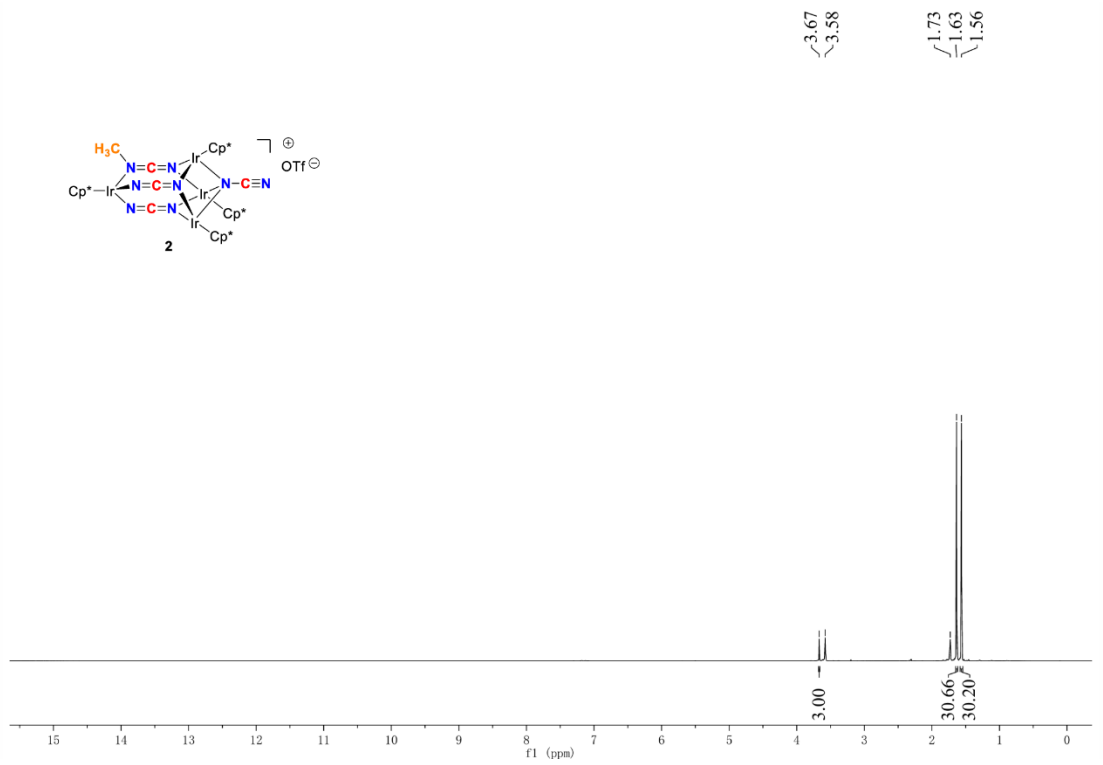

Figure S2. ^{1}H NMR spectrum of **2** (25 °C, 400 MHz, d_8-THF).

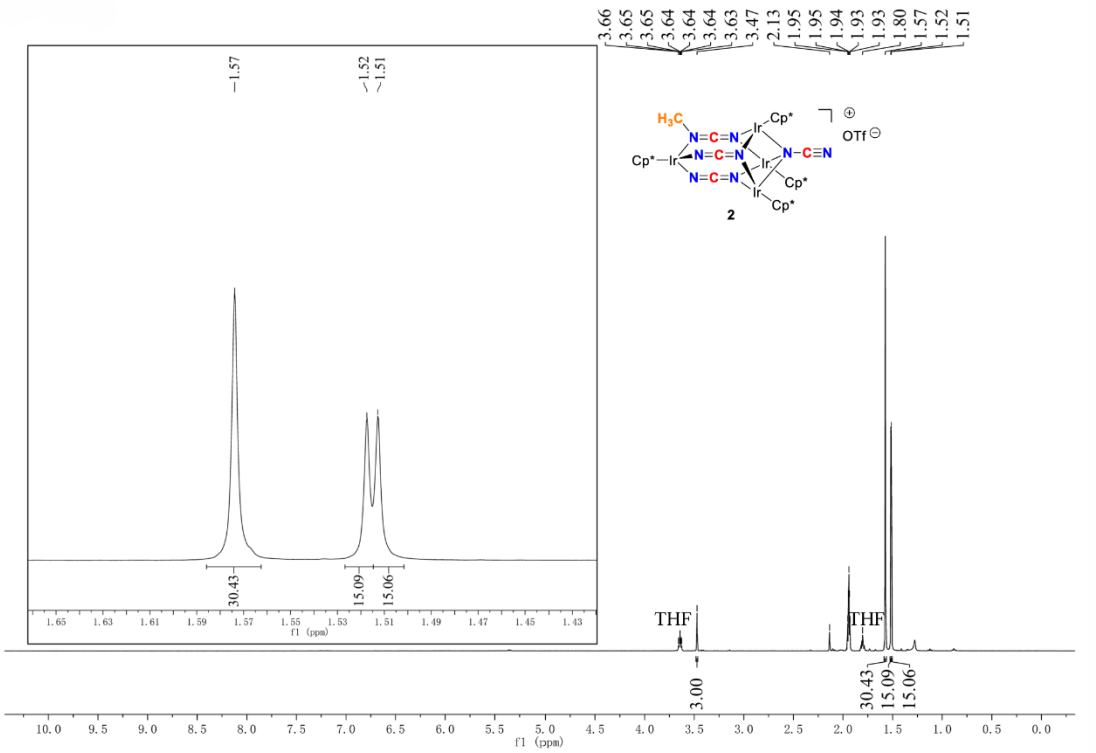

Figure S3. ^{1}H NMR spectrum of **2** (25 °C, 400 MHz, CD_3CN).

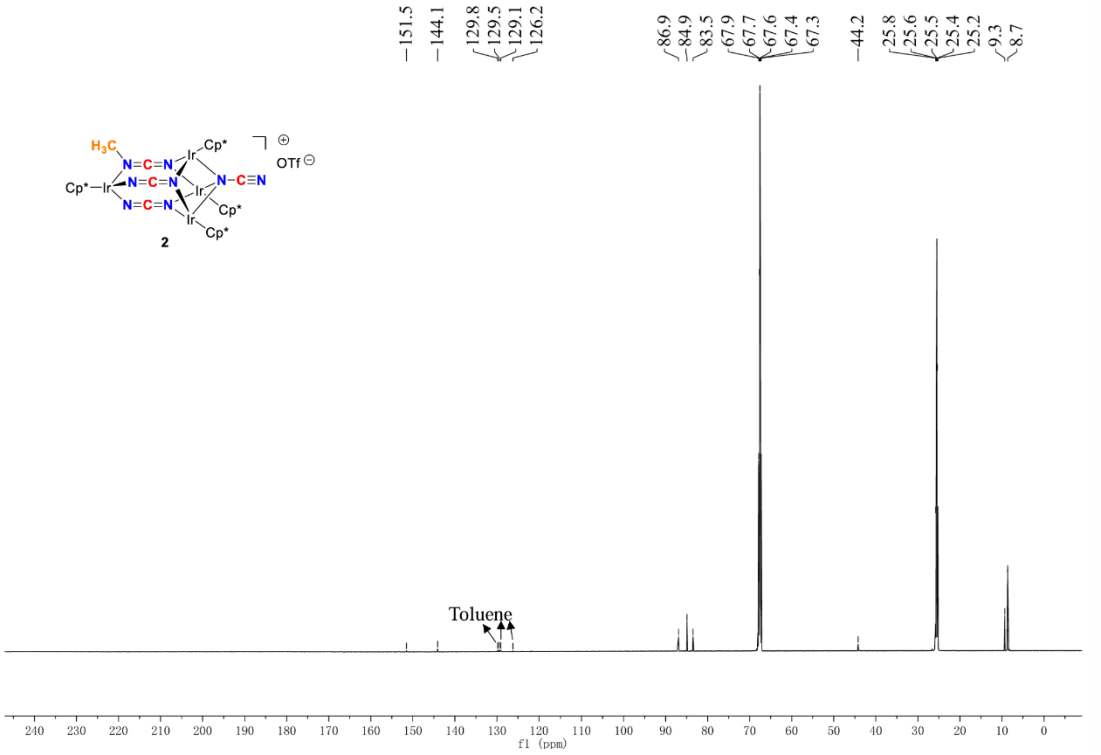

Figure S4. $^{13}C\{^{1}H\}$ NMR spectrum of **2** (25 °C, 151 MHz, d_8-THF).

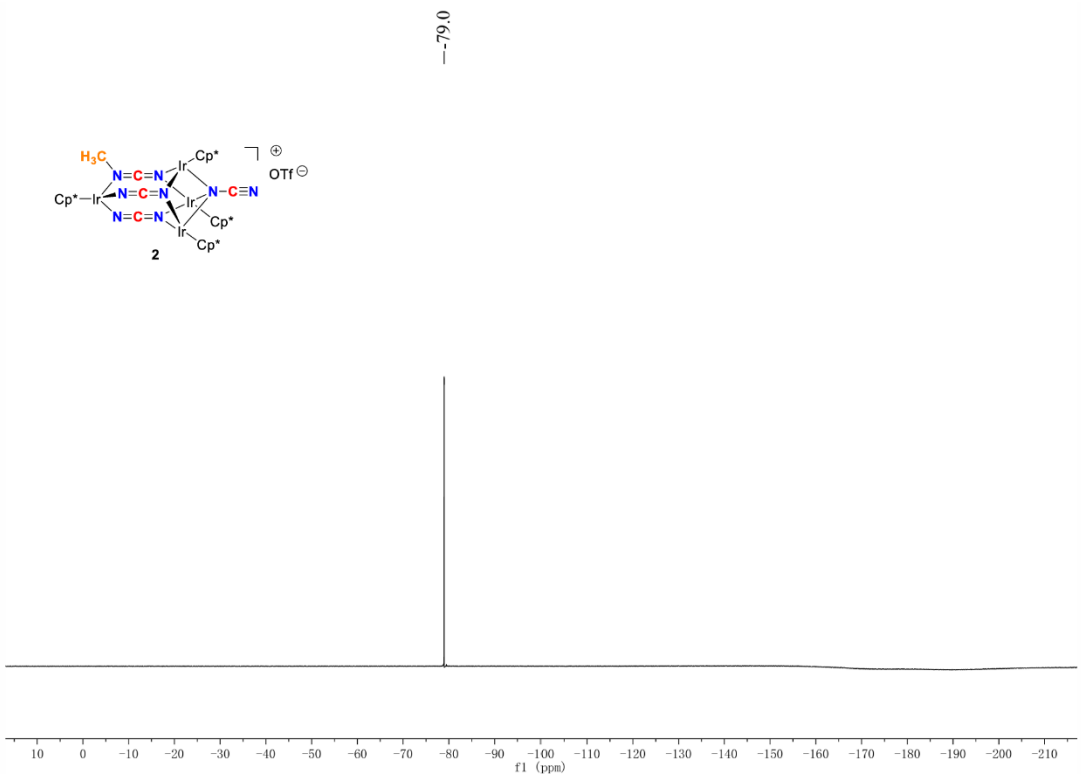

Figure S5. ^{19}F NMR spectrum of **2** (25 °C, 471 MHz, d_8-THF).

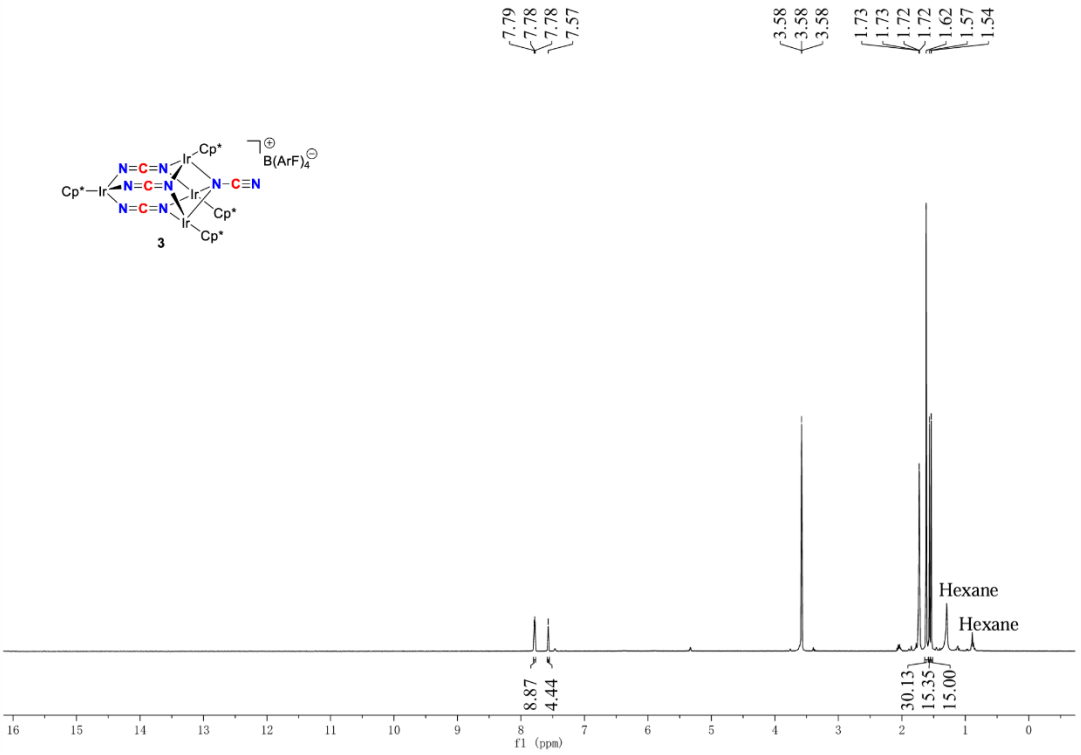

Figure S6. ^{1}H NMR spectrum of **3** (25 °C, 600 MHz, d_8-THF).

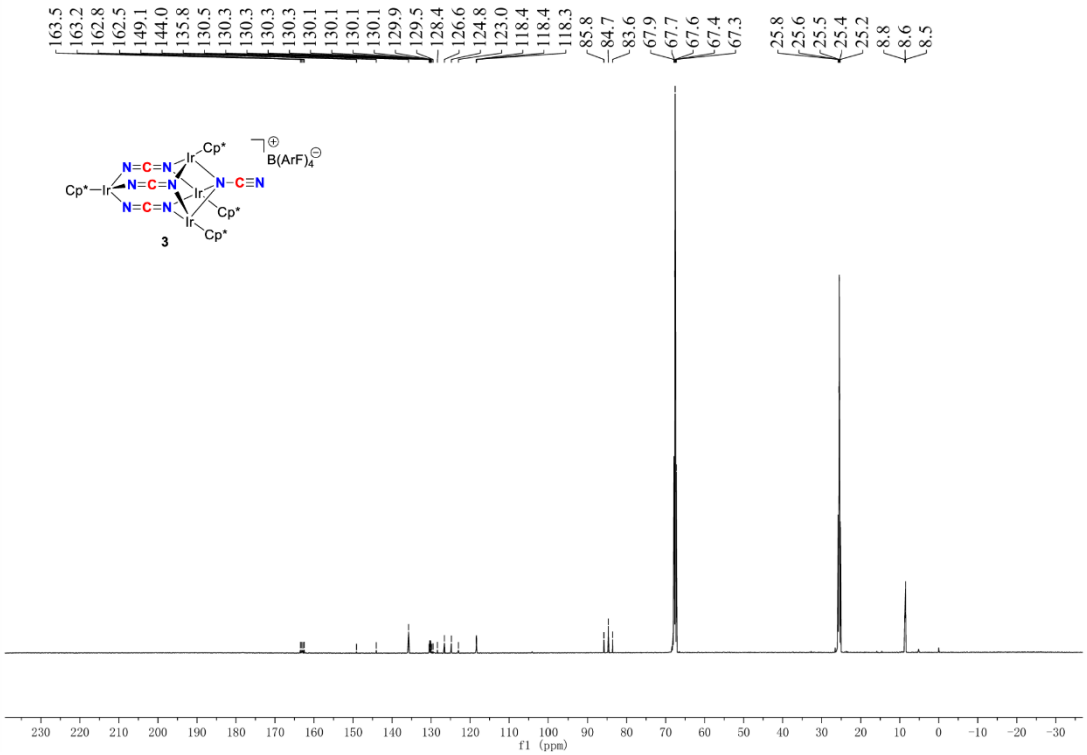

Figure S7. $^{13}C\{^{1}H\}$ NMR spectrum of **3** (25 °C, 151 MHz, d_8-THF).

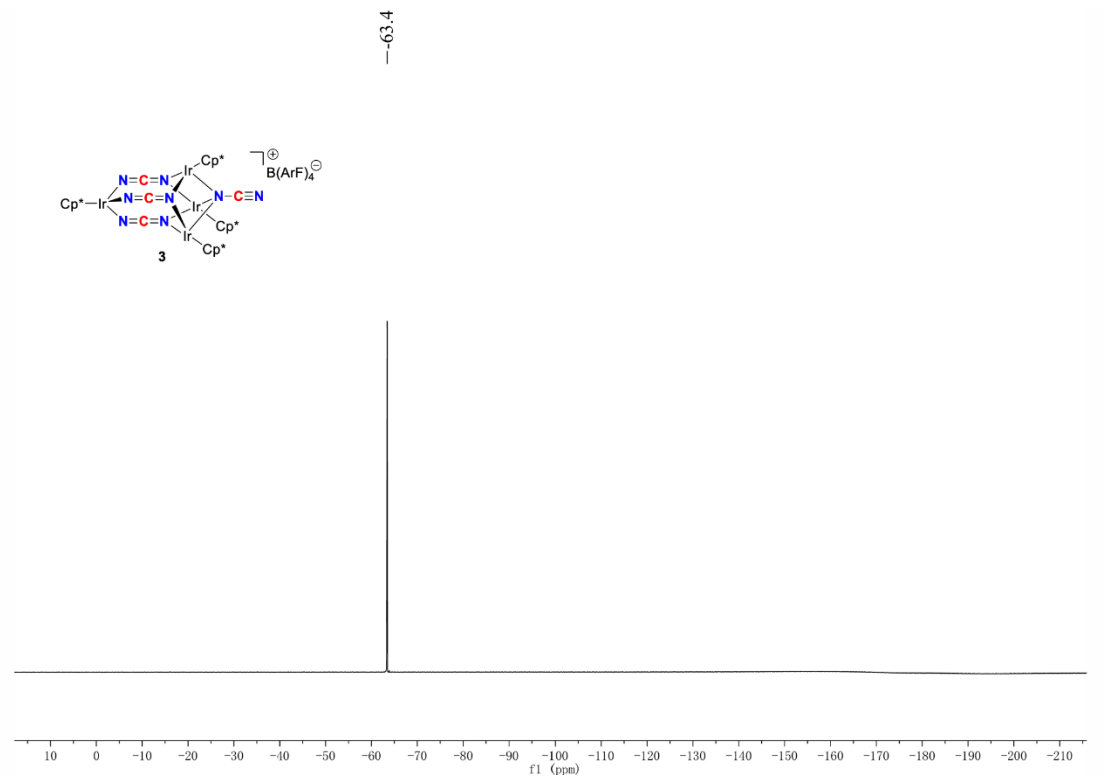

Figure S8. ^{19}F NMR spectrum of **3** (25 °C, 471 MHz, d_8-THF).

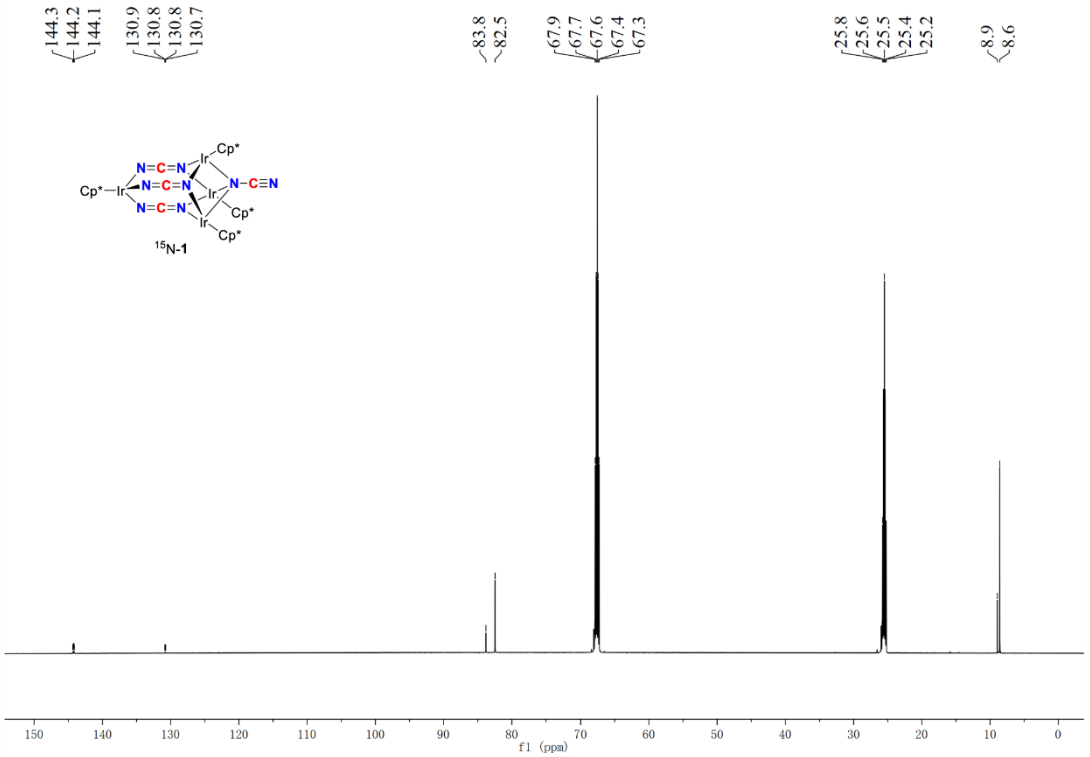

Figure S9. $^{13}C\{^{1}H\}$ NMR spectrum of ^{15}N-**1** (25 °C, 151 MHz, d_8-THF).

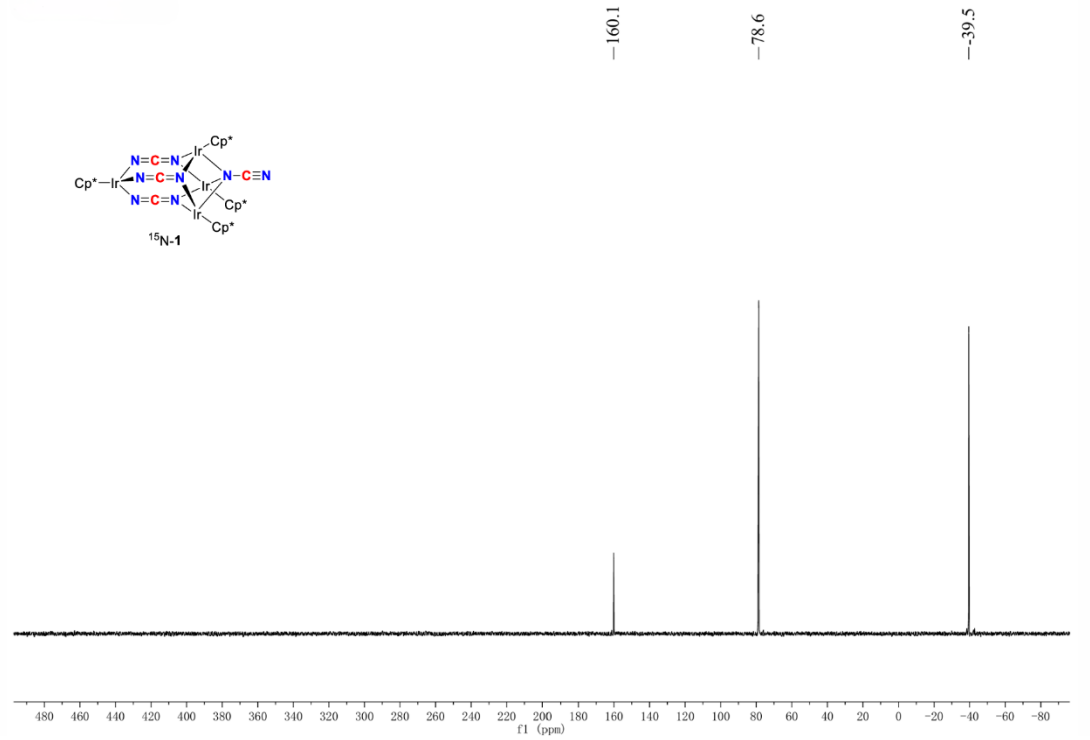

Figure S10. ^{15}N NMR spectrum of ^{15}N-**1** (25 °C, 61 MHz, d_8-THF).

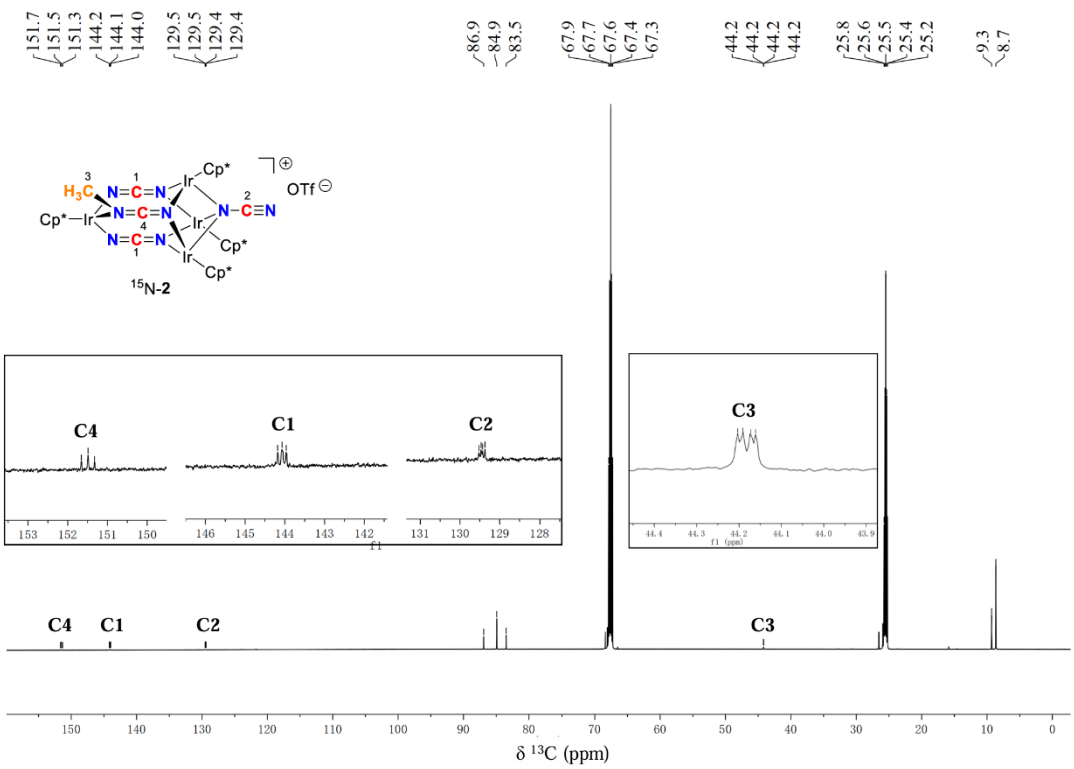

Figure S11. $^{13}C\{^{1}H\}$ NMR spectrum of ^{15}N-**2** (25 °C, 151 MHz, d_8-THF).

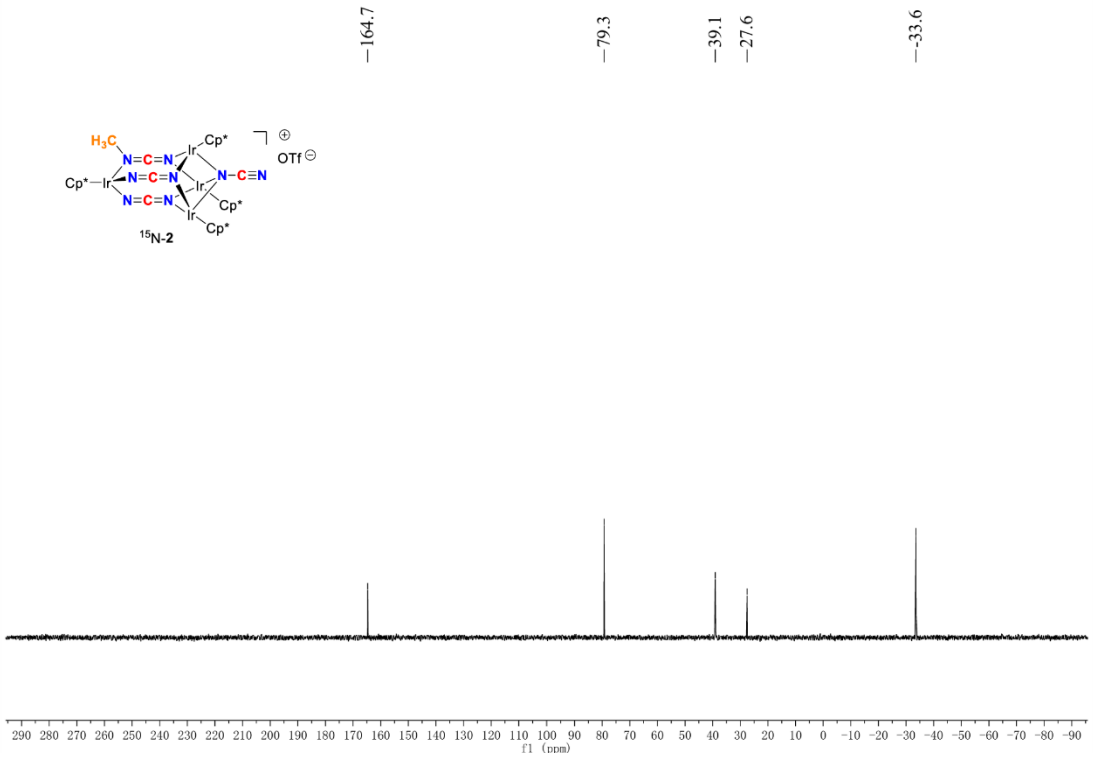

Figure S12. ^{15}N NMR spectrum of ^{15}N-**2** (25 °C, 61 MHz, d_8-THF).

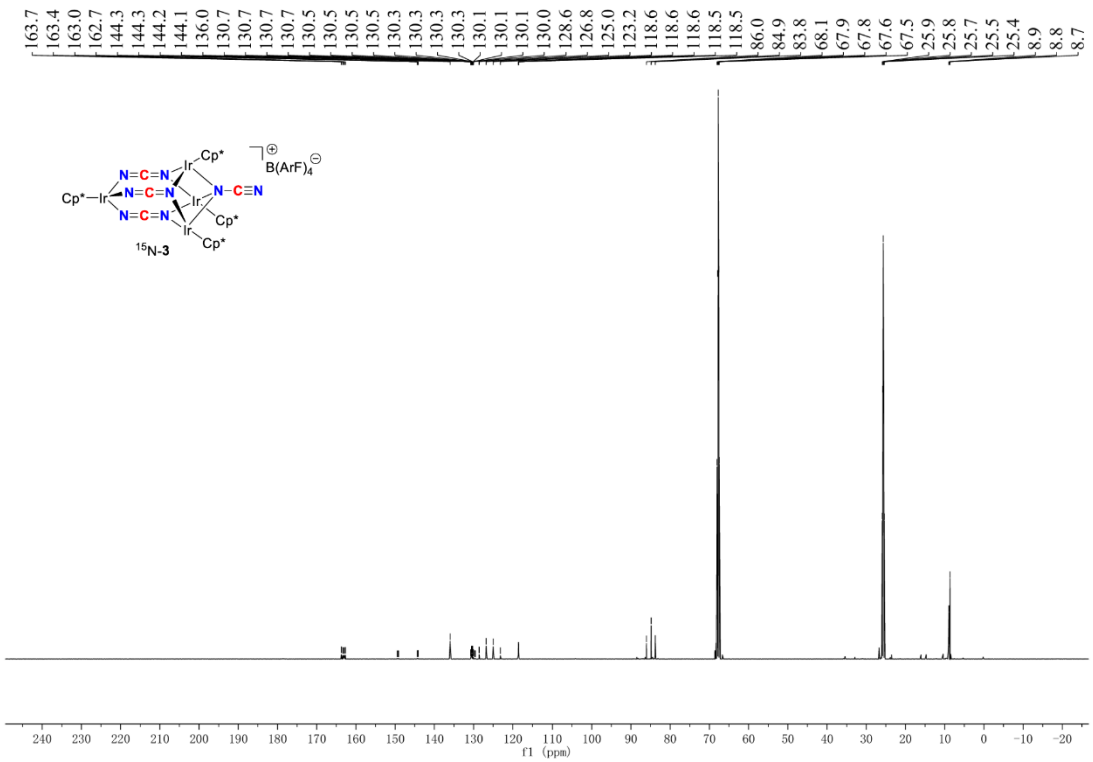

Figure S13. $^{13}C\{^{1}H\}$ NMR spectrum of ^{15}N-**3** (25 °C, 151 MHz, d_8-THF).

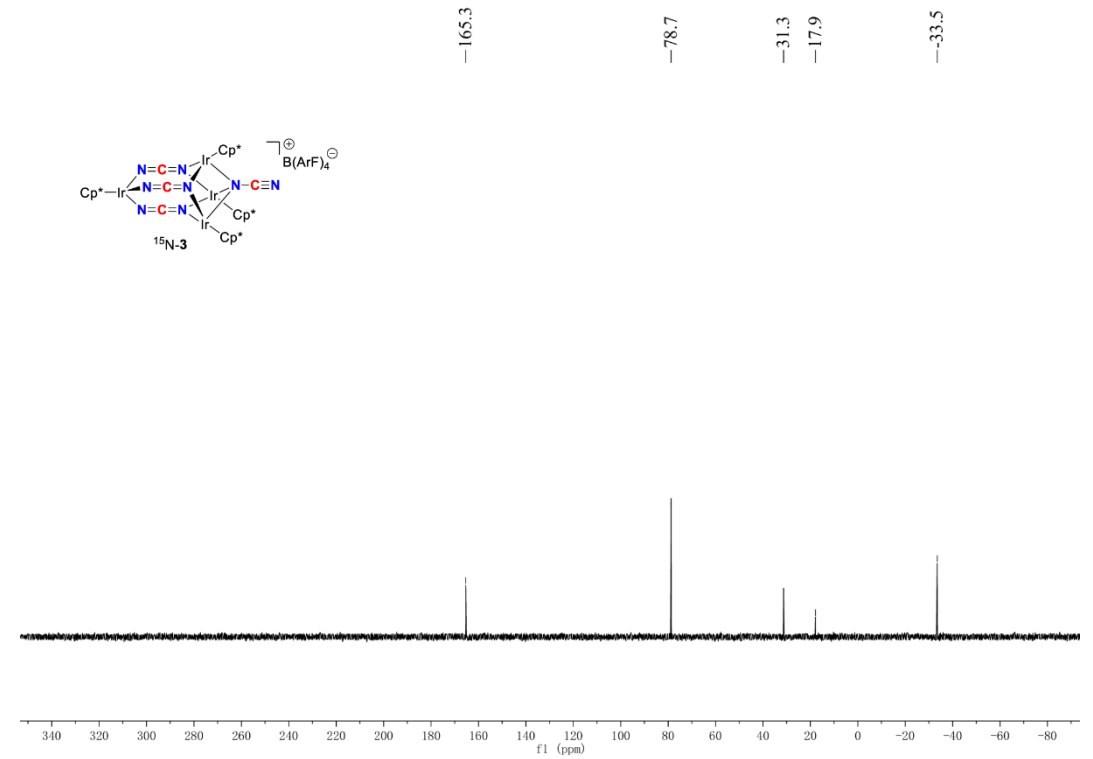

Figure S14. ^{15}N NMR spectrum of ^{15}N-**3** (25 °C, 61 MHz, d_8-THF).

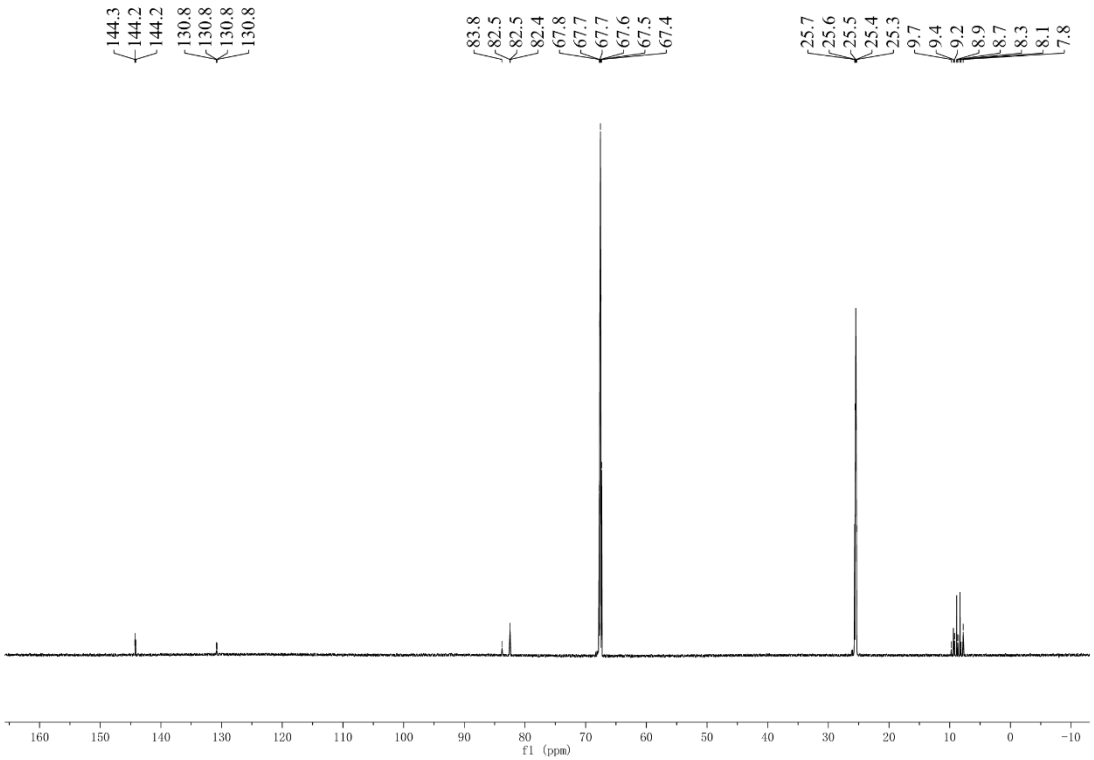

Figure S15. $^{13}C\{^{1}H\}$ NMR spectrum of ^{15}N-**1** (25 °C, 239 MHz, d_8-THF, proton-coupled).

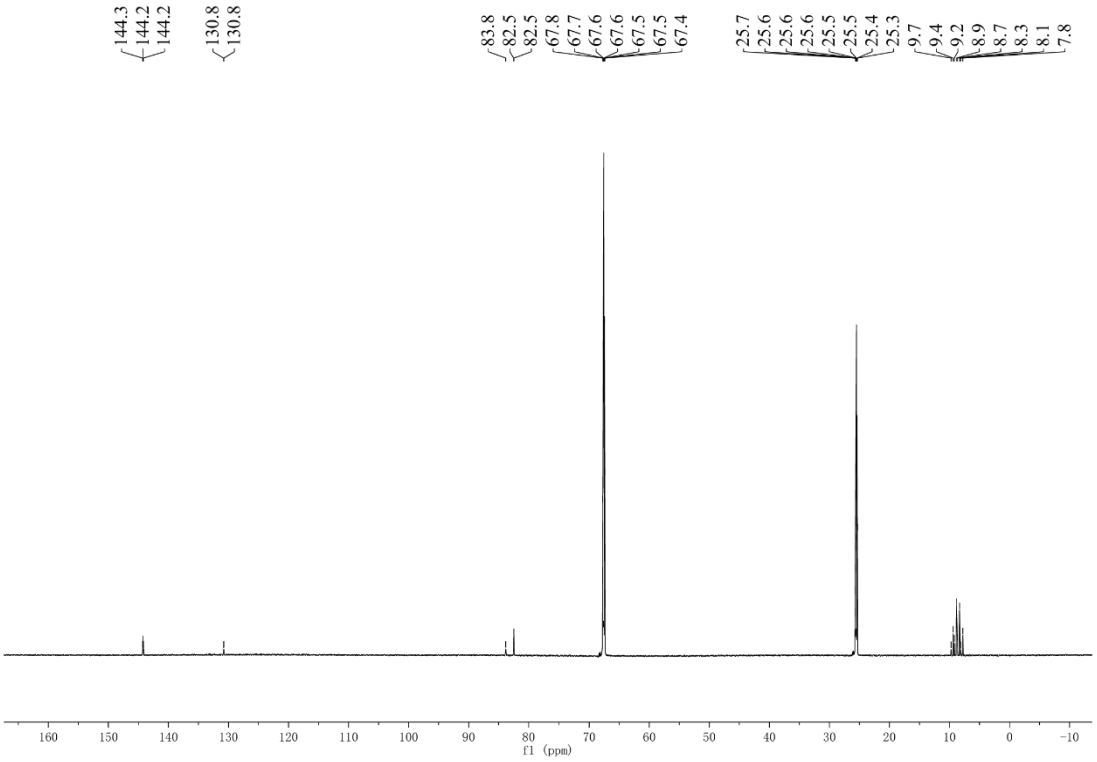

Figure S16. ^{13}C NMR spectrum of ^{15}N-**1** (25 °C, 239 MHz, d_8-THF, proton-coupled, selective decoupling of the ^{15}N signal at 160.1 ppm).

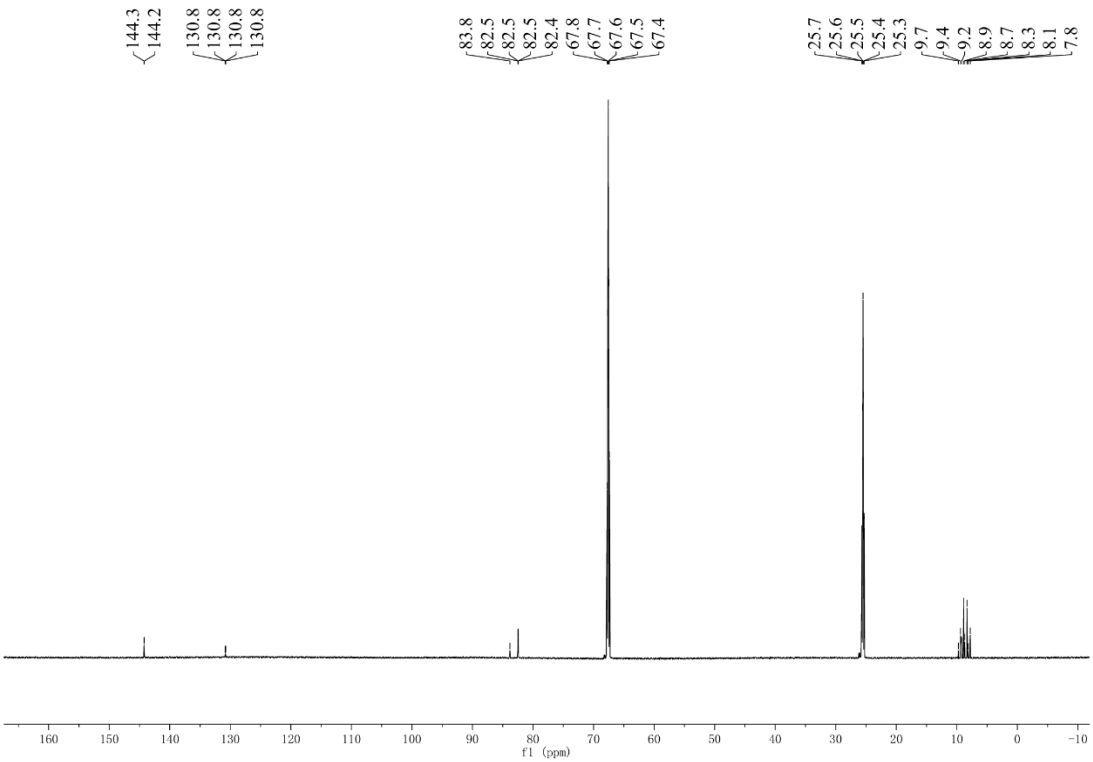

Figure S17. ^{13}C NMR spectrum of ^{15}N-**1** (25 °C, 239 MHz, d_8-THF, proton-coupled, selective decoupling of the ^{15}N signal at 78.6 ppm).

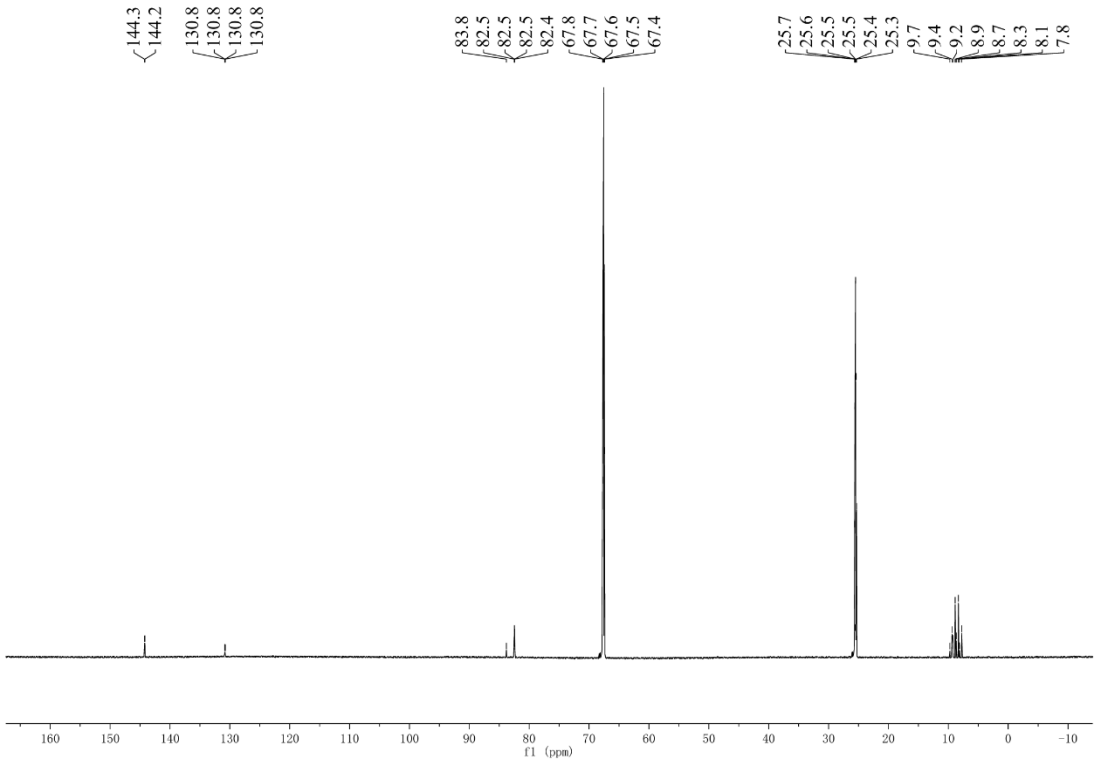

Figure S18. ^{13}C NMR spectrum of ^{15}N-**1** (25 °C, 239 MHz, d_8-THF, proton-coupled, selective decoupling of the ^{15}N signal at -39.5 ppm).

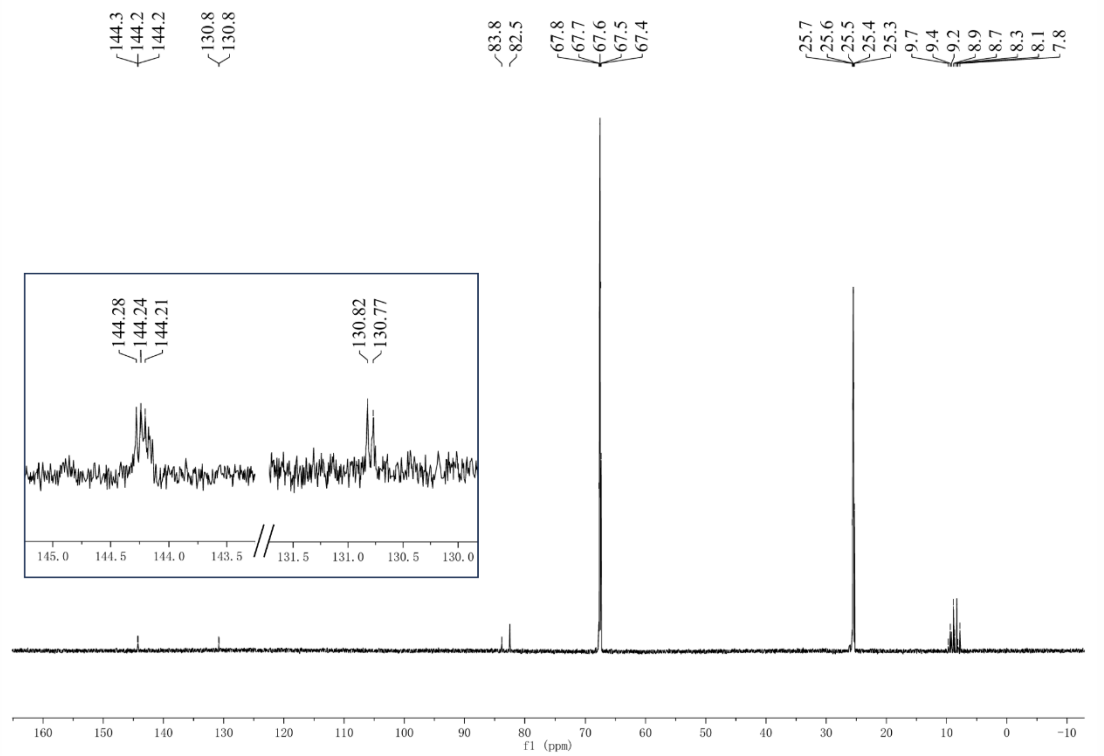

Figure S19. ^{13}C NMR spectrum of ^{15}N-**1** (25 °C, 239 MHz, d_8-THF, proton-coupled, selective decoupling of the ^{15}N signal at -170 ppm).

2) Copies of IR Spectra

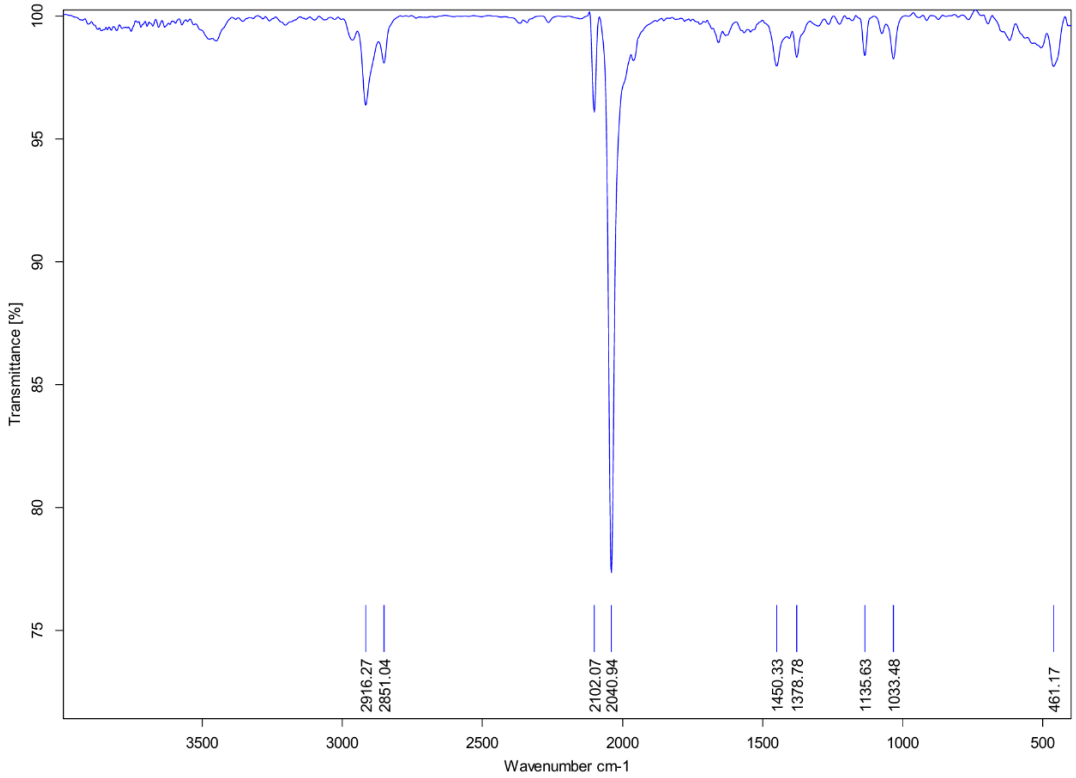

Figure S20. IR spectrum of **1** in KBr pellet at room temperature.

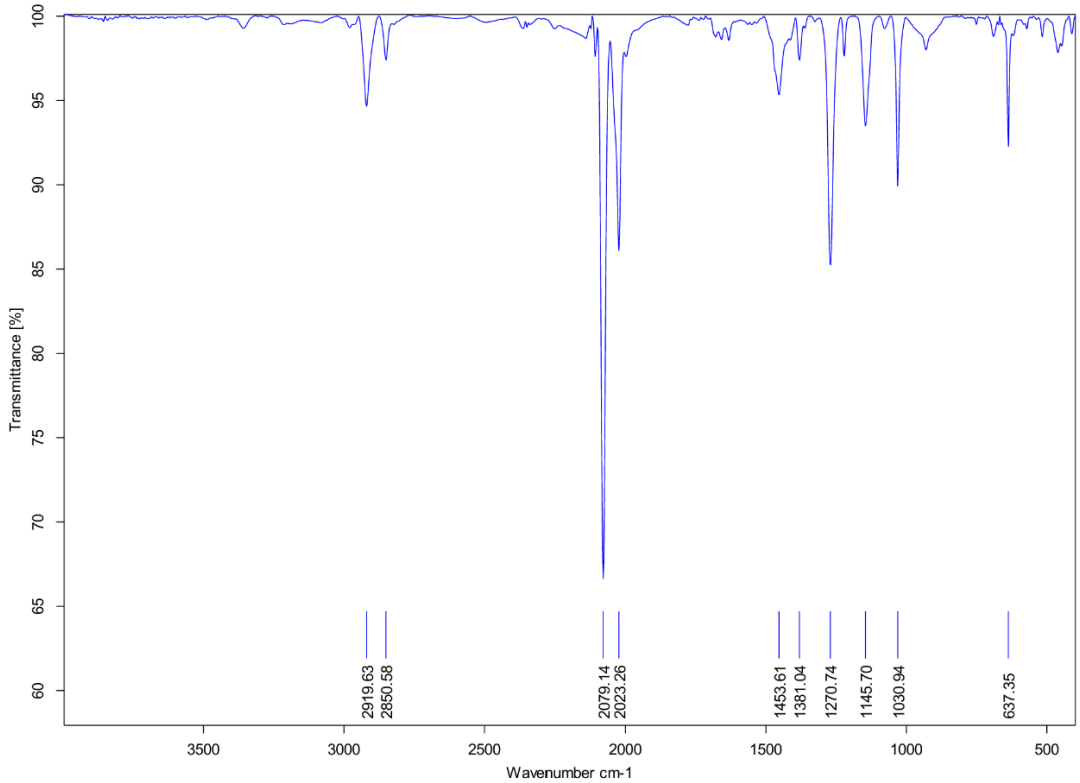

Figure S21. IR spectrum of **2** in KBr pellet at room temperature.

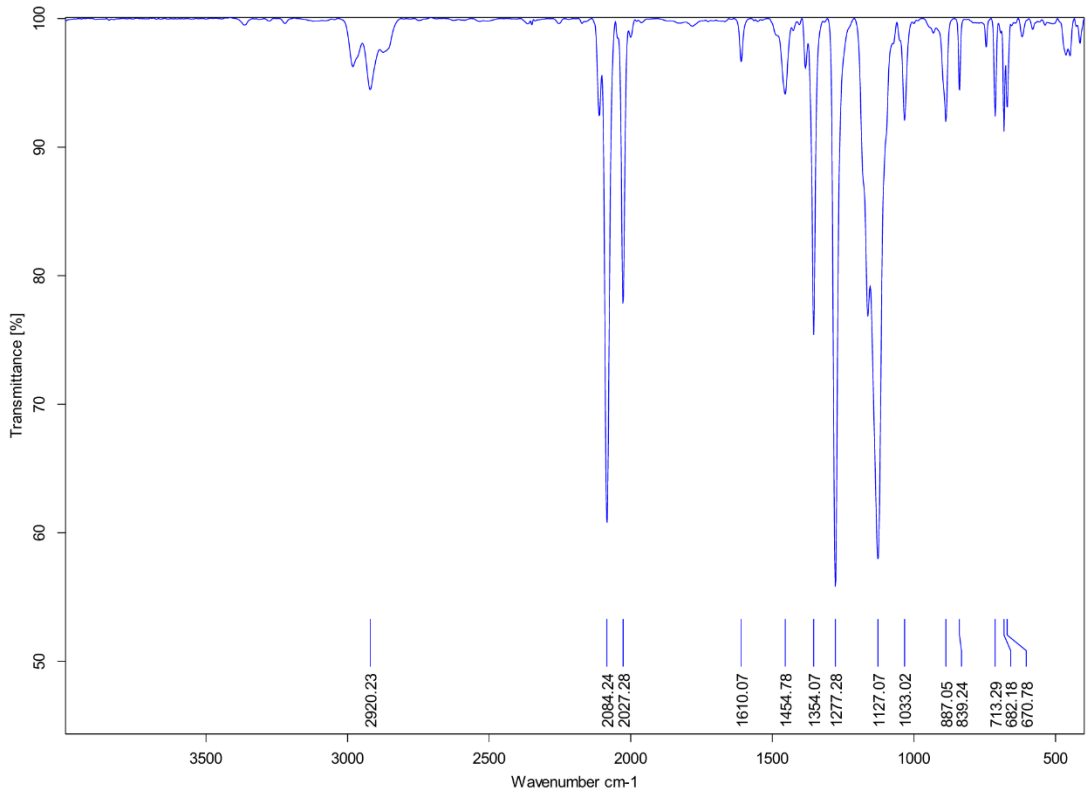

Figure S22. IR spectrum of **3** in KBr pellet at room temperature.

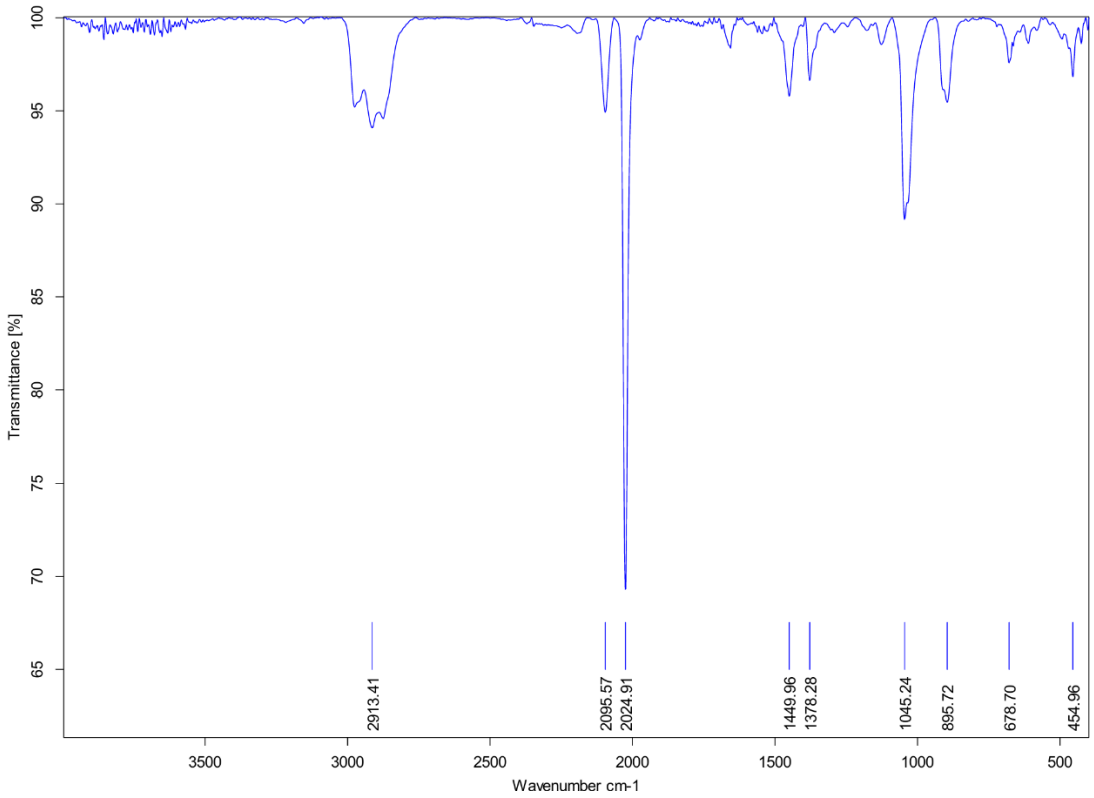

Figure S23. IR spectrum of ^{15}N-**1** in KBr pellet at room temperature.

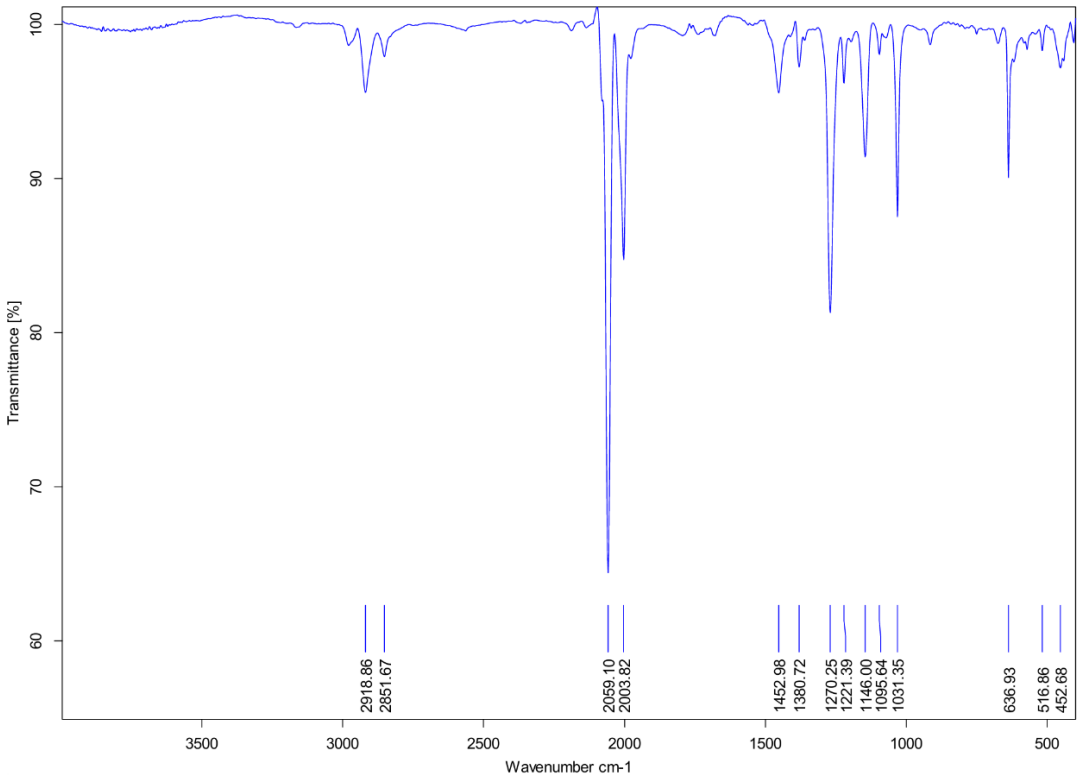

Figure S24. IR spectrum of ^{15}N-**2** in KBr pellet at room temperature.

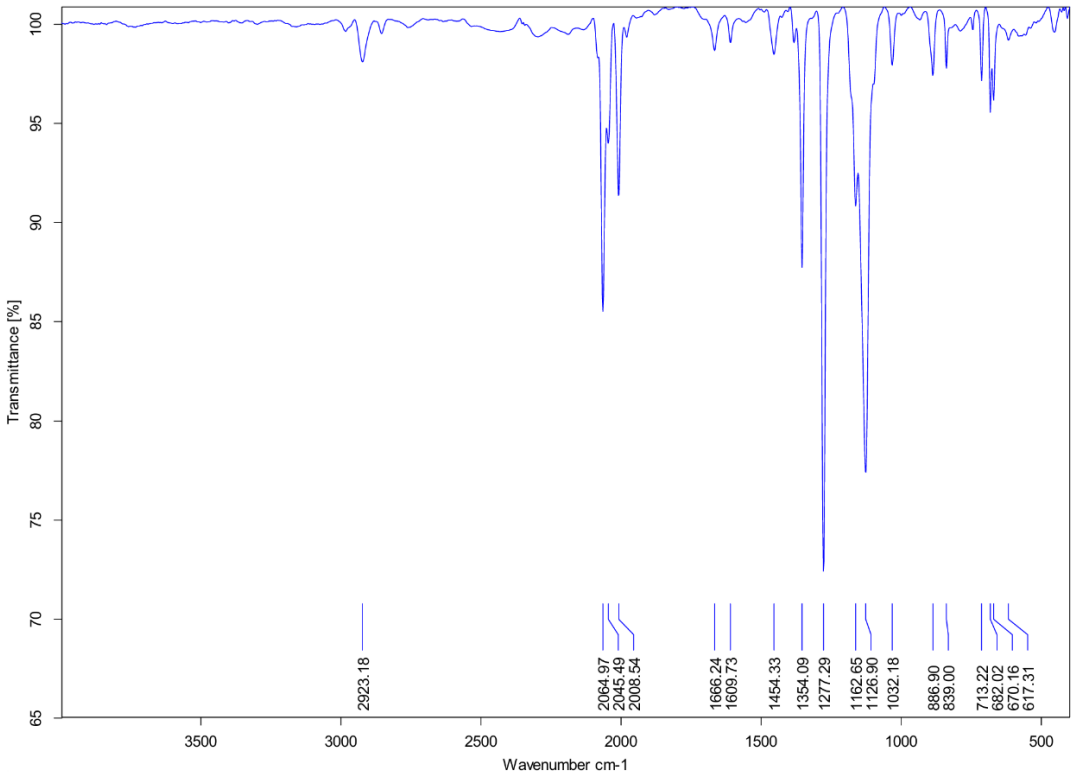

Figure S25. IR spectrum of ^{15}N-**3** in KBr pellet at room temperature.

3) Copies of ESI-MS Spectra

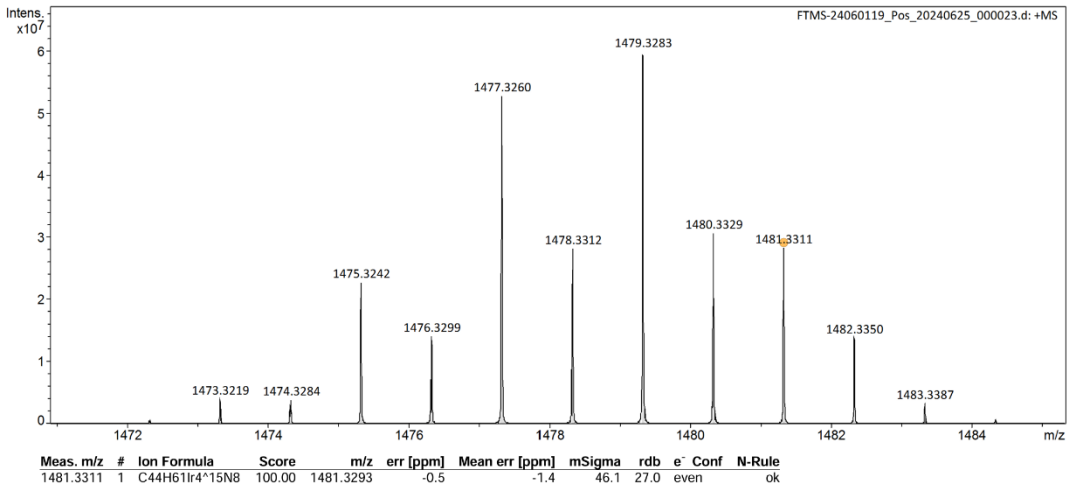

Figure S26. ESI-MS spectrum of ^{15}N-**1**.

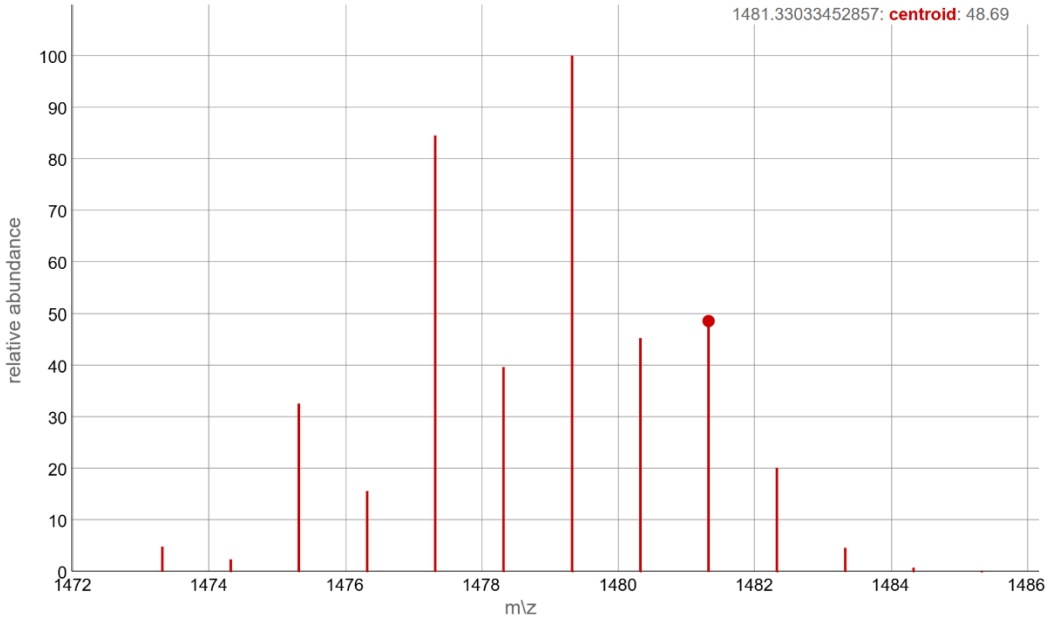

Figure S27. ESI-MS spectrum simulation of ^{15}N-**1**.

[^{15}N-**1** + H]$^+$ Chemical Formula: $C_{44}H_{61}Ir_4{}^{15}N_8{}^+$

m/z: 1479.33 (100.0%), 1477.33 (84.7%), 1481.33 (48.2%), 1480.33 (43.8%), 1478.33 (39.7%), 1475.32 (32.1%), 1482.33 (18.2%), 1476.33 (15.6%), 1473.32 (4.8%), 1483.34 (4.5%), 1474.32 (2.3%), 1482.34 (1.9%), 1480.34 (1.4%)

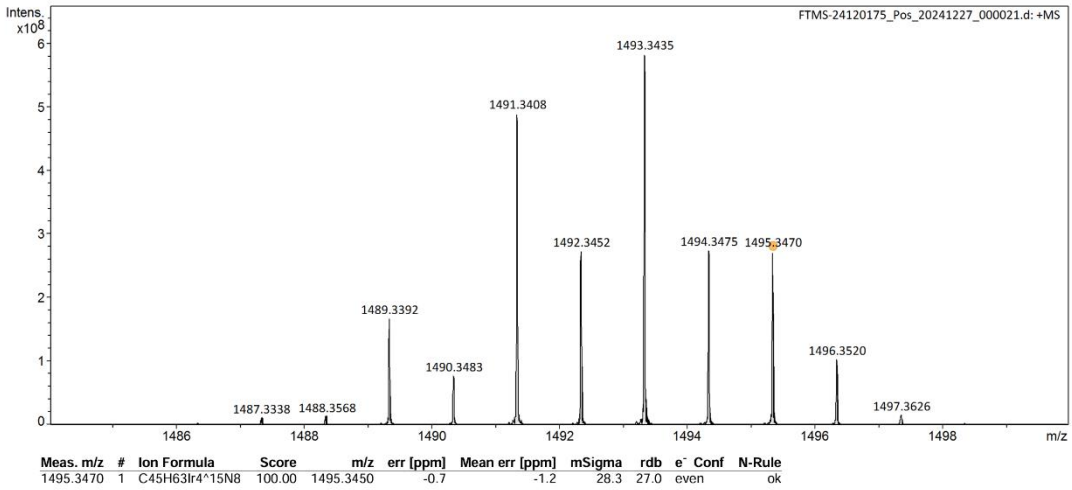

Figure S28. ESI-MS spectrum of ^{15}N-**2**.

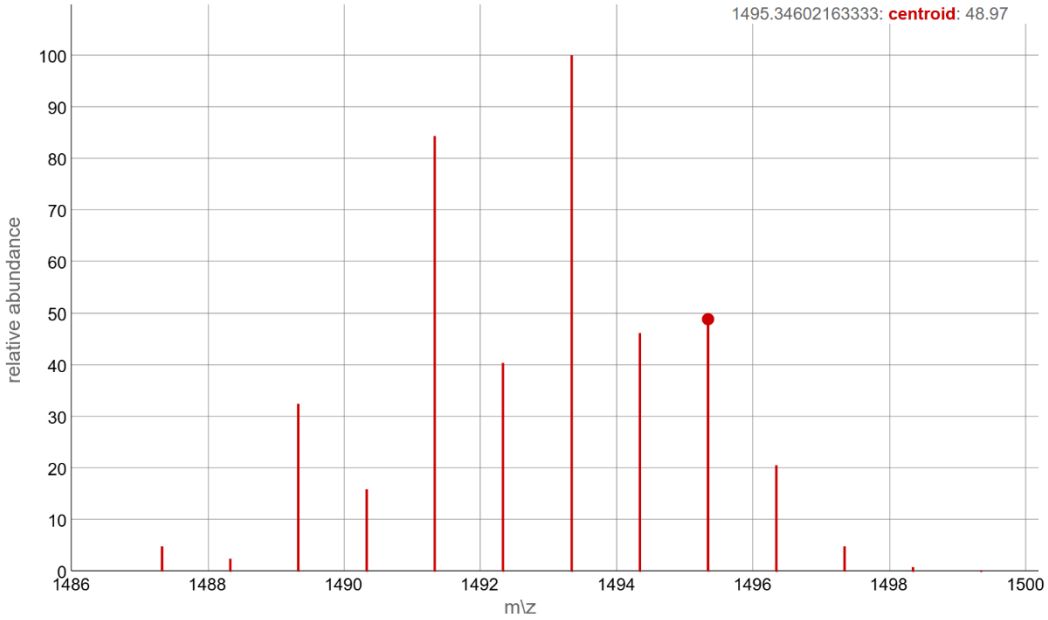

Figure S29. ESI-MS spectrum simulation of ^{15}N-**2**.

[^{15}N-**2** − OTf]$^{+}$ Chemical Formula: $C_{45}H_{63}Ir_4{}^{15}N_8{}^{+}$

m/z: 1493.34 (100.0%), 1491.34 (89.2%), 1495.35 (54.1%), 1494.35 (51.1%), 1492.34 (43.4%), 1489.34 (36.0%), 1496.35 (22.6%), 1490.34 (17.5%), 1493.35 (10.7%), 1487.34 (5.3%), 1497.35 (4.9%), 1491.35 (4.2%), 1488.34 (2.6%), 1492.35 (1.3%)

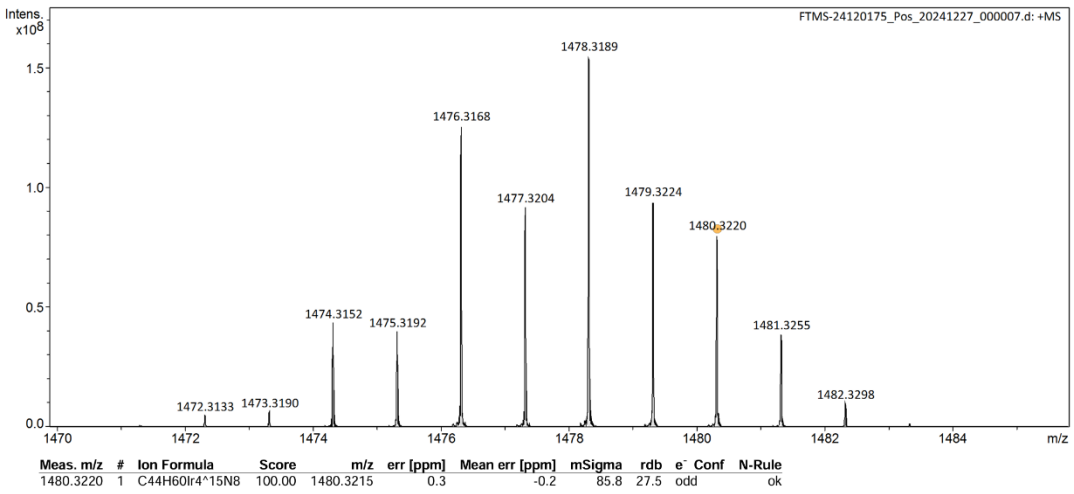

Figure S30. ESI-MS spectrum of ^{15}N-**3**.

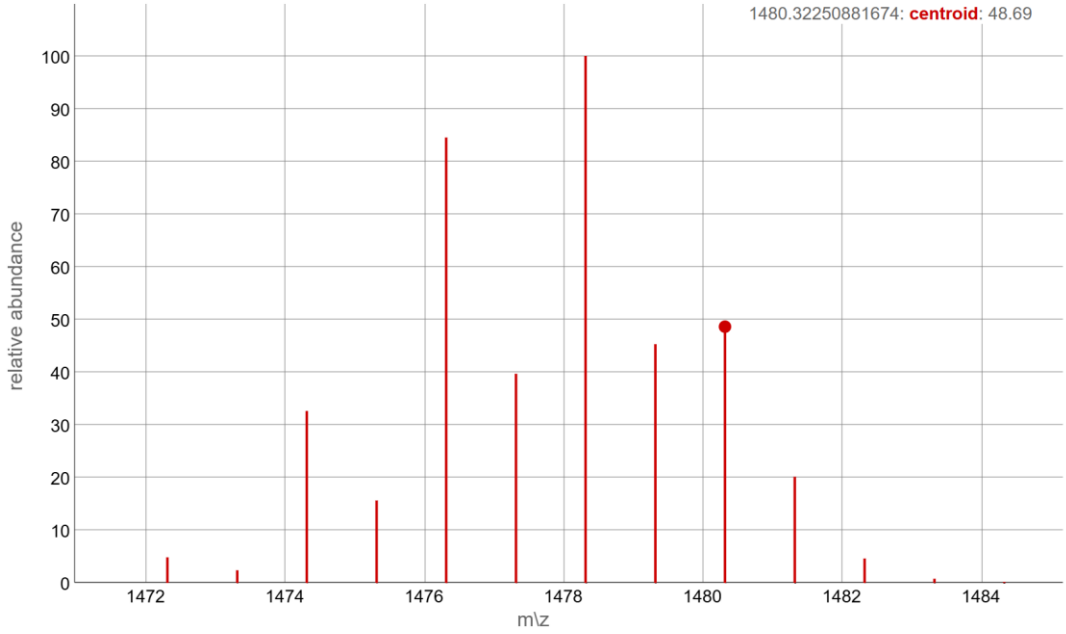

Figure S31. ESI-MS spectrum simulation of ^{15}N-**3**.

[^{15}N-**3** – B(ArF)$_4$]$^+$ Chemical Formula: $C_{44}H_{60}Ir_4{}^{15}N_8{}^+$

m/z: 1478.32 (100.0%), 1476.32 (84.9%), 1479.32 (43.3%), 1477.32 (39.2%), 1480.32 (38.2%), 1474.32 (32.8%), 1481.33 (20.1%), 1475.32 (15.6%), 1480.33 (10.5%), 1472.31 (4.8%), 1482.33 (4.5%), 1473.32 (2.3%), 1479.33 (2.1%)

4) X-ray Crystallographic Studies

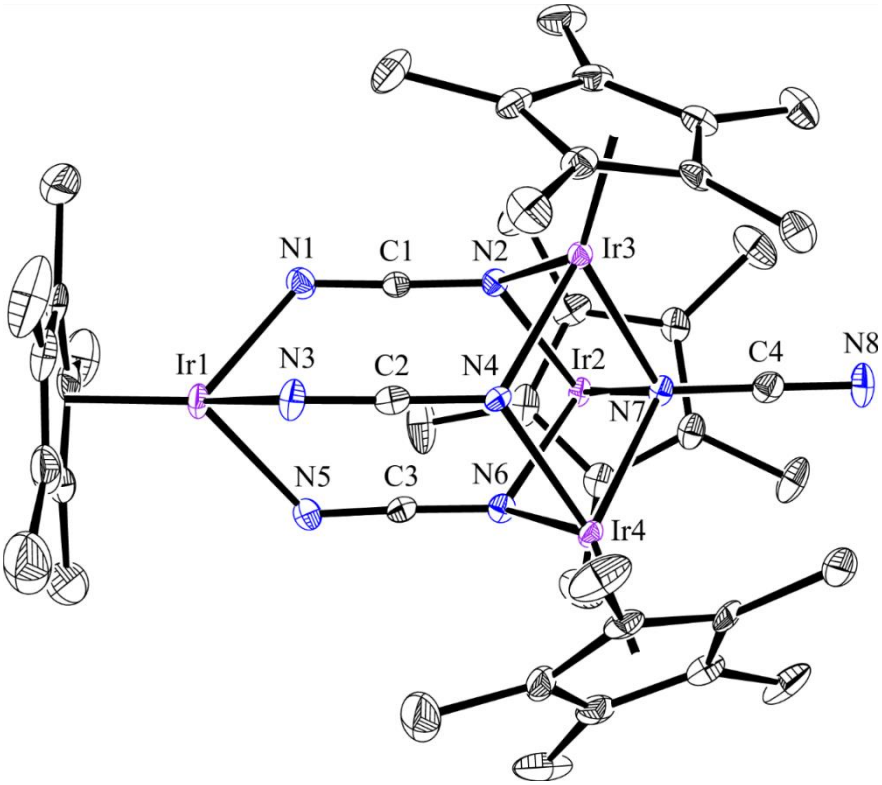

Figure S32. ORTEP drawing of **1**. Thermal ellipsoids are shown at the 30% probability level. Hydrogen atoms are omitted for clarity. Selected bond lengths (Å) and angles (deg): Ir1−N1 2.109(5), Ir1−N3 2.113(6), Ir1−N5 2.109(6), Ir2−N2 2.090(5), Ir2−N6 2.096(5), Ir2−N7 2.157(5), Ir3−N2 2.096(5), Ir3−N4 2.097(5), Ir3−N7 2.170(5), Ir4−N4 2.098(5), Ir4−N6 2.095(5), Ir4−N7 2.165(5), N1−C1 1.206(8), N2−C1 1.244(8), N3−C2 1.186(8), N4−C2 1.255(8), N5−C3 1.193(8), N6−C3 1.260(8), N7−C4 1.323(8), N8−C4 1.164(8), N1−C1−N2 177.6(7), N3−C2−N4 176.5(7), N5−C3−N6 177.2(7), N7−C4−N8 179.3(8).

Table S1 X-ray crystallographic data for **1**

Identification code	2412180
Empirical formula	$C_{96}H_{141}Ir_8N_{16}O_2$
Formula weight	3088.84
Temperature/K	180.00(10)
Crystal system	monoclinic

Space group	$P2_1/n$
a/Å	34.1212(7)
b/Å	17.7347(3)
c/Å	16.6640(3)
α/°	90
β/°	101.540(2)
γ/°	90
Volume/Å^3	9880.0(3)
Z	4
ρ_{calc} g/cm^3	2.077
μ/mm^{-1}	10.784
F(000)	5844.0
Crystal size/mm^3	0.2 × 0.1 × 0.1
Radiation	MoKα (λ = 0.71073)
2Θ range for data collection/°	4.458 to 54.968
Index ranges	-44 ≤ h ≤ 42, -22 ≤ k ≤ 23, -20 ≤ l ≤ 20
Reflections collected	74256
Independent reflections	22574 [R_{int} = 0.0260, R_{sigma} = 0.0327]
Data/restraints/parameters	22574/726/1146
Goodness-of-fit on F^2	1.028
Final R indexes [I>=2σ (I)]	R_1 = 0.0344, wR_2 = 0.0645
Final R indexes [all data]	R_1 = 0.0547, wR_2 = 0.0708
Largest diff. peak/hole / e Å^{-3}	3.17/-2.34

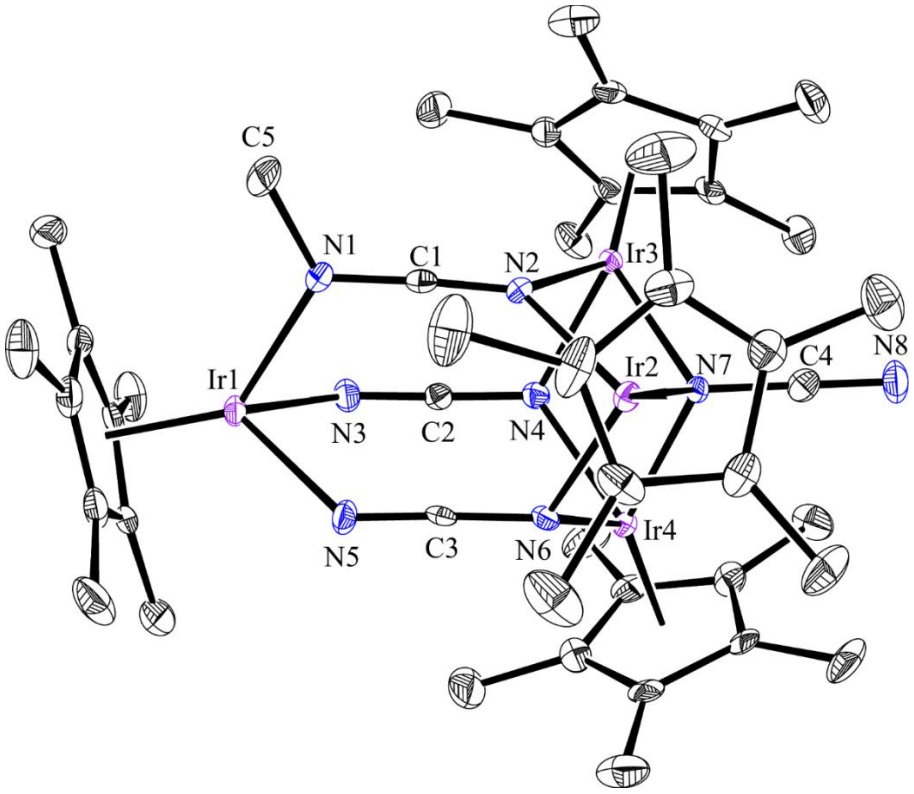

Figure S33. ORTEP drawing of **2**. Thermal ellipsoids are shown at the 30% probability level. Hydrogen atoms and OTf anion are omitted for clarity. Selected bond lengths (Å) and angles (deg): Ir1−N1 2.176(6), Ir1−N3 2.102(6), Ir1−N5 2.109(5), Ir2−N2 2.149(5), Ir2−N6 2.107(5), Ir2−N7 2.152(5), Ir3−N2 2.134(5), Ir3−N4 2.088(5), Ir3−N7 2.163(5), Ir4−N4 2.100(5), Ir4−N6 2.106(5), Ir4−N7 2.194(5), N1−C1 1.246(8), N2−C1 1.203(8), N3−C2 1.192(8), N4−C2 1.259(8), N5−C3 1.181(8), N6−C3 1.273(8), N7−C4 1.336(8), N8−C4 1.156(9), N1−C5 1.484(9), N1−C1−N2 176.4(7), N3−C2−N4 176.9(7), N5−C3−N6 176.5(7), N7−C4−N8 179.6(9).

Table S2 X-ray crystallographic data for **2**

Identification code	2412205
Empirical formula	$C_{99}H_{134}F_6Ir_8N_{16}O_6S_2$
Formula weight	3359.93
Temperature/K	180.00(10)
Crystal system	triclinic

Space group	*P-1*
a/Å	13.2902(4)
b/Å	20.7356(6)
c/Å	22.0373(6)
α/°	68.321(3)
β/°	85.575(2)
γ/°	75.402(3)
Volume/Å^3	5460.4(3)
Z	2
ρ_{calc} g/cm^3	2.044
μ/mm^{-1}	9.813
F(000)	3180.0
Crystal size/mm^3	0.2 × 0.1 × 0.1
Radiation	MoKα (λ = 0.71073)
2Θ range for data collection/°	4.256 to 54.964
Index ranges	-17 ≤ h ≤ 17, -26 ≤ k ≤ 26, -28 ≤ l ≤ 26
Reflections collected	103632
Independent reflections	24981 [R_{int} = 0.0514, R_{sigma} = 0.0452]
Data/restraints/parameters	24981/936/1350
Goodness-of-fit on F^2	1.049
Final R indexes [I>=2σ (I)]	R_1 = 0.0355, wR_2 = 0.0880
Final R indexes [all data]	R_1 = 0.0522, wR_2 = 0.0940
Largest diff. peak/hole / e Å^{-3}	2.97/-2.23

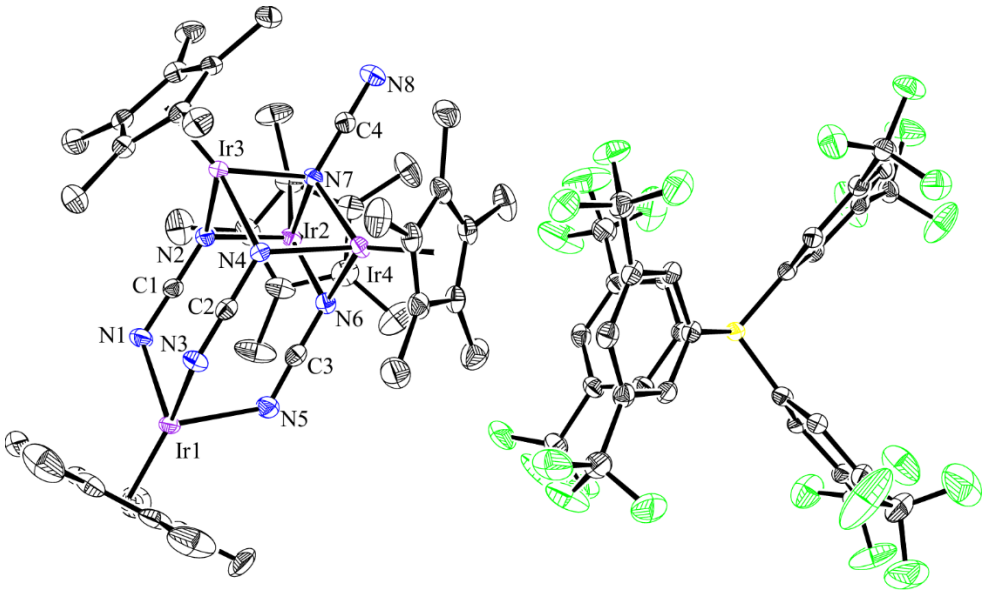

Figure S34. ORTEP drawing of **3**. Thermal ellipsoids are shown at the 30% probability level. Hydrogen atoms are omitted for clarity. Selected bond lengths (Å) and angles (deg): Ir1−N1 2.109(6), Ir1−N3 2.122(6), Ir1−N5 2.111(6), Ir2−N2 2.104(6), Ir2−N6 2.095(6), Ir2−N7 2.160(5), Ir3−N2 2.102(5), Ir3−N4 2.100(5), Ir3−N7 2.144(6), Ir4−N4 2.088(5), Ir4−N6 2.105(6), Ir4−N7 2.162(5), N1−C1 1.207(9), N2−C1 1.247(9), N3−C2 1.180(9), N4−C2 1.292(9), N5−C3 1.208(9), N6−C3 1.238(9), N7−C4 1.329(9), N8−C4 1.156(10), N1−C1−N2 179.2(8), N3−C2−N4 177.4(7), N5−C3−N6 177.3(8), N7−C4−N8 179.6(9).

Table S3 X-ray crystallographic data for **3**

Identification code	2412208
Empirical formula	$C_{76}H_{72}BF_{24}Ir_4N_8$
Formula weight	2333.02
Temperature/K	180.00(10)
Crystal system	orthorhombic
Space group	$P2_12_12_1$
a/Å	19.3731(2)

b/Å	19.4020(2)
c/Å	20.8027(2)
α/°	90
β/°	90
γ/°	90
Volume/Å^3	7819.25(14)
Z	4
ρ_{calc} g/cm^3	1.982
μ/mm^{-1}	6.892
F(000)	4452.0
Crystal size/mm^3	0.2 × 0.1 × 0.1
Radiation	MoKα (λ = 0.71073)
2Θ range for data collection/°	4.198 to 54.968
Index ranges	-25 ≤ h ≤ 25, -25 ≤ k ≤ 25, -27 ≤ l ≤ 27
Reflections collected	248315
Independent reflections	17921 [R_{int} = 0.0546, R_{sigma} = 0.0238]
Data/restraints/parameters	17921/0/1038
Goodness-of-fit on F^2	1.056
Final R indexes [I>=2σ (I)]	R_1 = 0.0250, wR_2 = 0.0517
Final R indexes [all data]	R_1 = 0.0308, wR_2 = 0.0540
Largest diff. peak/hole / e Å^{-3}	1.72/-0.61

5) The Cyclic Voltammetry of 1

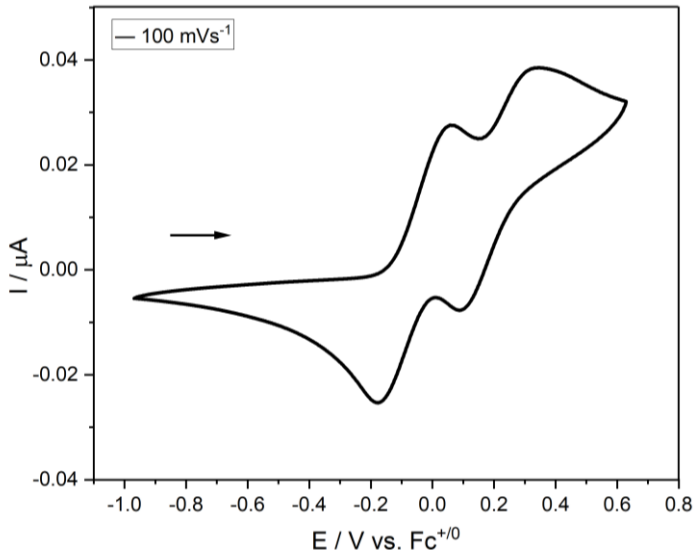

Figure S35. Cyclic voltammogram of **1**. Conditions: 1.0 mM in 0.10 M [^{n}Bu$_4$N][PF$_6$] /THF under argon, room temperature; Platinum electrodes working electrode; scan rate, 100 mVs^{-1}.

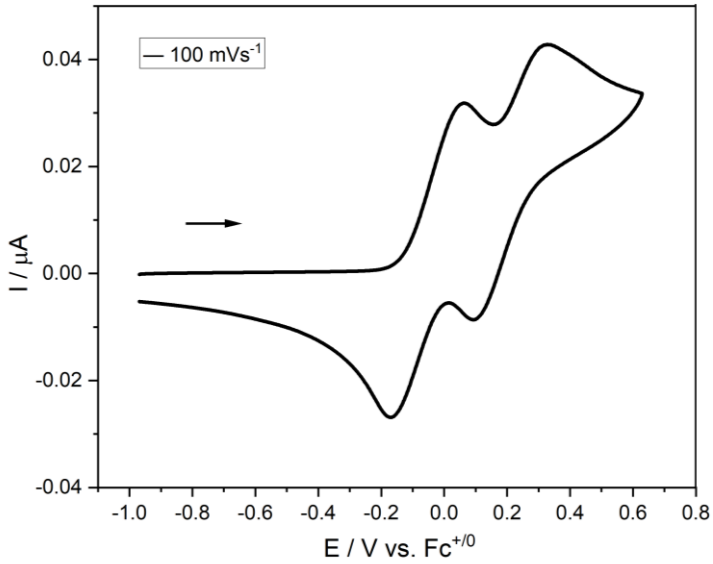

Figure S36. The first cycle of cyclic voltammogram of complex **1**. Conditions: 1.0 mM in 0.10 M [^{n}Bu$_4$N][PF$_6$] /THF under argon, room temperature; Platinum electrodes working electrode; scan rate, 100 mVs^{-1}.

6) Copies of EPR Spectra

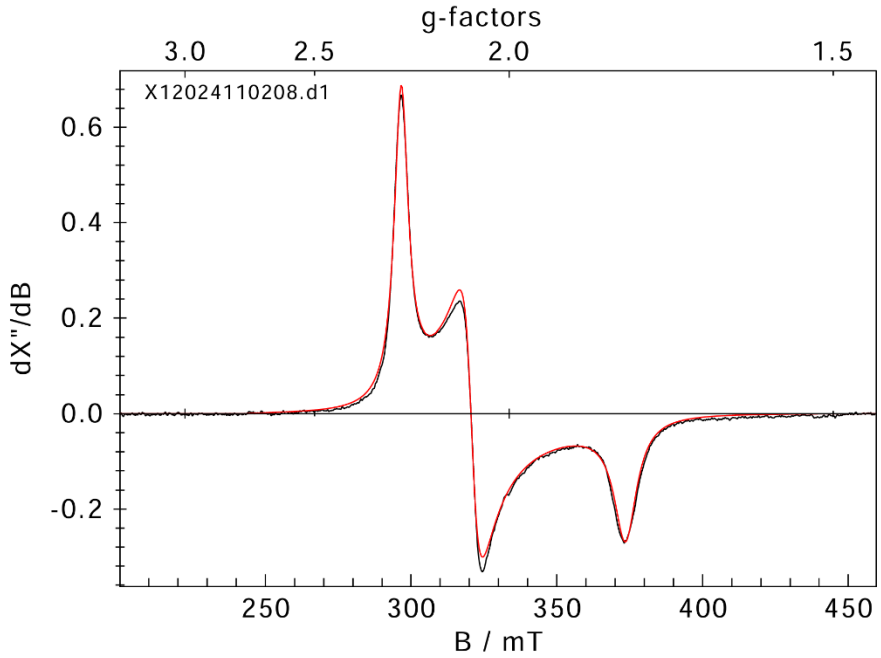

Figure S37. X-band EPR spectrum (blackline) and simulation (redline) of a 5mM THF solution of **3**. Acquisition conditions: temperature = 114.7 K, microwave power = 1.01 mW and modulation amplitude = 2 G. Simulation parameters: g_x = 2.249, g_y = 2.080, g_z = 1.786.

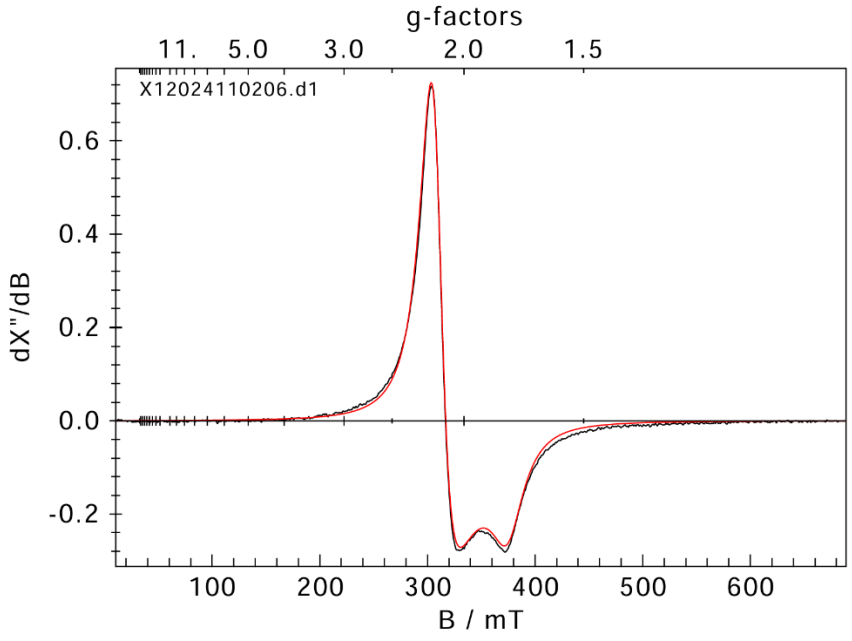

Figure S38. X-band EPR spectrum (blackline) and simulation (redline) of **3** in solid. Acquisition conditions: temperature = 114.7 K, microwave power = 1.01 mW and modulation amplitude = 2 G. Simulation parameters: g_x = 2.162, g_y = 2.162, g_z = 1.781.

7) Computational Details

Density functional theory (DFT) calculations were performed using ORCA 6.0.0[1] to investigate the electronic structures of **1**, **2,** and **3**. The geometric structure was optimized at the TPSSh/def2-TZVP level of theory,[2] incorporating dispersion corrections via the Becke-Johnson damping scheme (D3BJ).[3] The optimized geometry closely matches the single-crystal structures, thereby validating the computational approach. To further ensure the accuracy of the results, single-point energy calculations were carried out on the optimized geometry using the double-hybrid functional PWPB95 and the def2-QZVPP basis sets.[4] The corresponding wavefunction analysis was performed using Multiwfn.[5]

We have carefully validated the spin state of **3**, ensuring that the computed electronic structure is physically meaningful. The optimized geometries were provided in the supplementary information dataset as .xyz files.

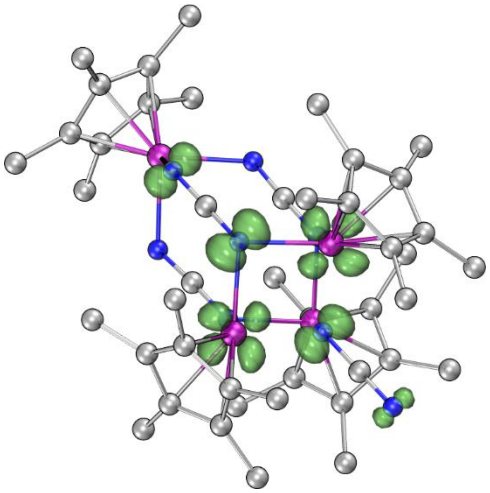

Figure S39. The spin density distribution of complex **3**. (The unpaired electron is primarily localized on the Ir3 and Ir4 atoms, contributing approximately 45%, determined by Fuzzy space partitioning.)

The IR calculation for complex **1** shows characteristic absorption peaks for the NCN units at 2043 cm^{-1} (the three-NCN set) and 2085 cm^{-1} (the single-NCN set), respectively. After methylation, the IR spectrum of complex **2** exhibits NCN peaks at 2019 cm^{-1}, 2070 cm^{-1} (the three-NCN set), and 2100 cm^{-1} (the single-NCN set). Upon oxidation, complex **3** displays NCN absorption bands at 2021 cm^{-1} (the three-NCN set) and 2097 cm^{-1} (the single-NCN set). These calculated IR results are in good agreement with the experimental data.

For the calculated IR analysis, based on the Database of Frequency Scale Factors for Electronic Model Chemistries, we applied a frequency scaling factor of 0.96.[6]

8) References

(1) F. Neese, *WIREs Comput. Mol. Sci*., 2022, **12**, e1606.

(2) J. P. Perdew, J. Tao, V. N. Staroverov and G. E. Scuseria, *J. Chem. Phys*., 2004, **120**, 6898-6911.

(3) S. Grimme, J. Antony, S. Ehrlich and H. Krieg, *J. Chem. Phys*., 2010, **132**, 154104.

(4) L. Goerigk and S. Grimme, *J. Chem. Theory Comput*., 2011, **7**, 291–309.

(5) T. Lu and F. Chen, *J. Comput. Chem*., 2012, **33**, 580–592.

(6) I. M. Alecu, J. Zheng, Y. Zhao and D. G. Truhlar, *J. Chem. Theory Comput.*, 2010, **6**, 2872-2887.